Three Periods of Drying of a Single Square Capillary Tube

F. Chauvet,[1] P. Duru,[1] S. Geoffroy,[2] and M. Prat[1,*]

[1]*Université de Toulouse; INPT, UPS; IMFT, Avenue Camille Soula, 31400 Toulouse, France and CNRS; IMFT 31400, Toulouse, France*

[2]*Université de Toulouse; INSA, UPS; LGMT, 135, avenue de Rangueil, 31077 Toulouse, France*

(Received 30 April 2009; published 16 September 2009)

The drying kinetics of a porous medium is classically described in three main periods, which depend on the interplay between the external and internal mass transfers during evaporation. The first period is described as essentially depending on the external mass transfer, whereas the third period is dominated by the internal mass transfer. The second period is a crossover period. We show experimentally that a similar drying kinetics can be obtained from a much simpler system owing to the effect of corner liquid films: a capillary tube of square cross section.

DOI: 10.1103/PhysRevLett.103.124502 PACS numbers: 47.56.+r, 68.03.Fg

Drying of porous media is a process of particular importance in relation with many applications, including soil drying, recovery of volatile hydrocarbons from underground oil reservoirs, and drying in food, textile, and pharmaceutical industries. Although much progress has been made on drying thanks to invasion percolation concepts and pore network simulations, e.g., [1], the prediction of drying rate, and therefore of drying time, is still a challenge. It is now widely admitted that this difficulty stems largely from the effect of liquid films in grooves, crevices of roughness in the pore space [2,3]. The accurate description of drying in a system where these films have a major effect is therefore of great interest. Although a porous medium with its hierarchy of pore diameters and junction structures is clearly much more complex, the consideration of an individual channel has often proven to be a useful step in the understanding of transport phenomena in porous media. Our study is also of direct interest for microfluidic systems, e.g., [4], where square and rectangular channels are common. Also, we note that little has been done on the evaporation from a single capillary tube since the pioneering experiments of Stefan [5] for circular tubes. Here we show that evaporation in a square tube is much faster and dramatically different owing to the effect of corner films. The square tube drying kinetics is shown to resemble the drying curve of a porous medium, which is classically described in three main periods as follows [6]. During the first period, referred to as the constant rate period (CRP), the evaporation rate is essentially constant and controlled by the external demand (velocity and relative humidity in surrounding air). The last period, the receding front period (RFP), is characterized by an internal evaporation front receding into the porous medium whereas the intermediate period, the falling rate period (FRP), is a crossover period characterized by a significant drop in the drying rate. The aim of this work is to present a detailed description of the drying kinetics for our simple system. Interestingly, this description is consistent with the analysis presented in [7], where it was argued that the CRP for a usual porous medium could exist even in the absence of bulk liquid-gas interface at the surface pores provided that liquid films reach the porous medium surface.

The 10 cm long square capillary tube is made of borosilicate glass. The tube internal side length d and wall thickness are 1 and 0.2 mm, respectively. The tube internal corners are not sharp but rounded (Fig. 1). Measurements of the tube internal curvature radius r_0 from high magnified images of tube cross sections give $r_0 \approx 100\ \mu$m. The capillary tube is held vertically and glued directly to a syringe placed on a precision pump, allowing accurate filling of the tube by the liquid (here n-heptane or 2-propanol, two perfectly wetting liquids). This setup is

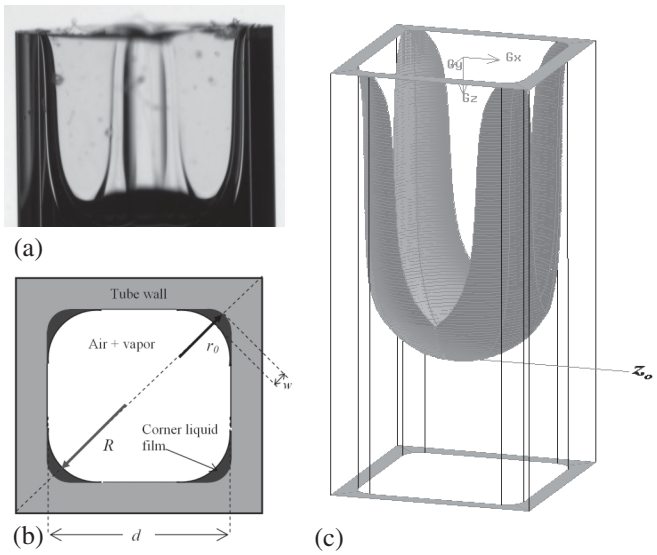

FIG. 1. (a) Visualization of corner liquid films in tube entrance [the camera is aligned on the tube diagonal axis (shown as a dashed line in (b)]. (b) Sketch of tube cross section in corner film region, where r_0 is the curvature radius of rounded corner, R is the in-plane curvature radius of corner menisci, and w is the corner film thickness. (c) Computed shape of gas-liquid interface in the tube.

placed inside a plexiglass enclosure which helps to maintain a constant temperature ($\pm 0.5\,^{\circ}$C) in the tube environment during the experiment. At $t = 0$, the top tube end is exposed to a stagnant air atmosphere at ambient temperature and evaporation starts. As shown in Fig. 1, thick liquid films remain trapped along the four internal corners when the bulk meniscus recedes into the tube as a result of evaporation. Using an ombroscopy visualization technique, images are acquired with two CCD cameras to follow both the bulk meniscus position z_0 and the evolution of corner films at the tube entrance.

The evolution of z_0 is shown in Fig. 2 together with its theoretical evolution for a circular tube for both liquids [5]. Evaporation is much faster with the square tube, for the corner films provide a pathway for transporting the liquid from the receding bulk meniscus up to the film tips. One can distinguish three main phases for the square tube: a first phase where z_0 seems to vary linearly with time, then a crossover period where the bulk meniscus significantly slows down, and eventually a third phase where $z_0 \propto \sqrt{t}$ as shown in the inset of Fig. 2. These three periods are best seen in Fig. 3, which shows the drying curve for the heptane experiment (a similar curve is obtained with the 2-propanol data). So as to use the same convention as for the drying curve of a porous medium [6], we define the liquid saturation as $S = (z_{0\max} - z_0)/z_{0\max}$, where $z_{0\max}$ is the farthest position reached by the bulk meniscus in the experiment. Hence S is the liquid volume fraction in the tube region $z \leq z_{0\max}$, neglecting, however, the small amount of liquid trapped along the corners. The evaporation flux E shown in Fig. 3 is estimated from the mass balance $E = \rho_\ell d^2(1 - A_c^*)\frac{dz_0}{dt}$, where ρ_ℓ is the liquid density and $A_c^* = \frac{4\lambda}{3.77^2}$ with $\lambda = 1 - \pi/4$. The area $d^2(1 - A_c^*)$ is the area left free of liquid within the tube as the junction between the bulk meniscus and the corner menisci for a perfectly wetting liquid [8]. Computing $\frac{dz_0}{dt}$ from our discrete series of data (t, z_0) is not straightforward because of the higher frequencies fluctuations of z_0 with time that are barely discernible in Fig. 2 but significantly affect the direct computation of derivatives from a simple finite difference scheme (these fluctuations are notably due to small temperature fluctuations and air motion variations induced by the room air conditioning system). One first option is to use a polynomial curve fitting procedure and compute $\frac{dz_0}{dt}$ from deriving the polynomial expression. This can be done splitting the data in several subsets and gives the solid line shown in Fig. 3, where $E_{\max}$ is the maximum evaporation flux computed using this procedure. An alternative consists in first applying a smoothing procedure to the raw data (t, z_0) and then computing $\frac{dz_0}{dt}$ using a simple finite difference scheme. We have tested several smoothing procedures (moving averages, Savitzky-Golay filters) and all give results consistent with the evolution deduced from the curve fitting procedure. An example of such results is

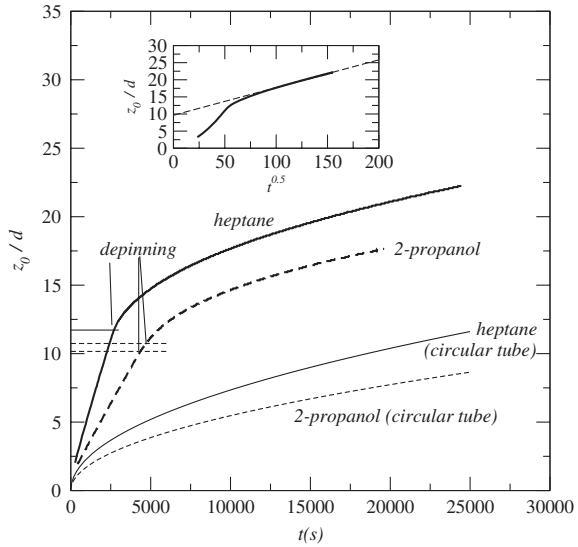

FIG. 2. Evolution of bulk meniscus position z_0 as a function of time. The thick solid line and the dashed line are for the square tube. The thin solid line and dashed line on the bottom are for a circular tube. The inset shows the evolution of z_0 as a function of $\sqrt{t}$ in the square tube with heptane. The position when the corner liquid films cease to be attached to the tube entrance (depinning) is indicated. The depinning does not occur at the same time in the four corners in the 2-propanol experiment. The two dashed lines indicate the first depinning and when depinning has occurred in the four corners, respectively.

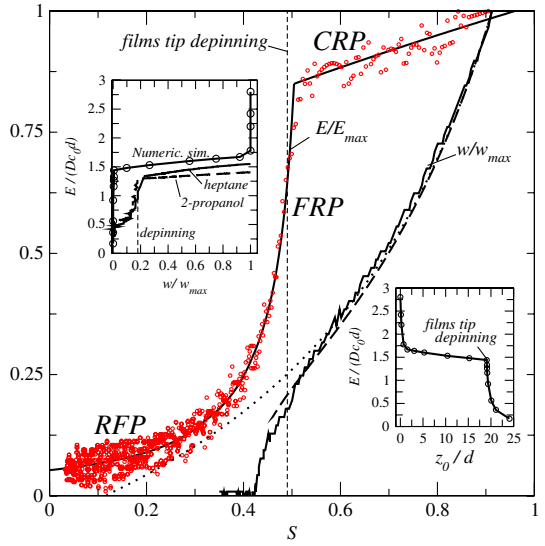

FIG. 3 (color online). Square tube drying kinetics with heptane [solid line from fits of $z_0(t)$, red circles from discrete derivatives, see text] and evolution of the corner film thickness w measured at a distance of one tube internal width d from tube entrance [solid line, the dotted line corresponds to the purely hydrostatic evolution, whereas the dashed line is deduced from a model of viscous flow in the film, see text, $w_{\max} = (\sqrt{2} - 1)(\frac{d}{3.77} - r_0)$]. The vertical dashed line marks the film tip depinning. The right-hand inset shows the drying kinetics as a function of z_0 computed numerically when the film thinning and depinning are due to gravity forces only. The left-hand inset shows the evolution of dimensionless evaporation flux as a function of w.

shown in Fig. 3 (circles). The remarkable result is that the drying curve in Fig. 3 is similar to the drying curve of porous media [6]. An accurate description of this curve is possible in relation with the evolution of film thickness w, measured inside the tube at a distance d from tube entrance from local visualization by ombroscopy, and also shown in Fig. 3 [w is the film thickness in the intersection between the corner angle bisector plane and the tube cross section plane; see Fig. 1(b)]. We now describe the three periods and how they are related to the external and internal mass transfers.

Figure 3 shows that the evaporation rate is not exactly constant but slowly decreases (almost linearly) during the CRP. Interestingly, this is also observed, but not explained, with porous media [6]. The observations indicate that the corner films are attached to the tube entrance and that the film thickness w decreases in the tube entrance region all along the CRP (Fig. 3). Hence the liquid is transported within the liquid films up to the tube entrance thanks to the effect of capillary forces during this period. The films' thinning induce, in turn, the slow decrease in the evaporation flux. The mechanisms responsible for the films' thinning can be understood from a simple model. Following [9], we express the liquid flow rate q within each of the four corner films as

$$q(z) = \rho_l \frac{\lambda R^4}{\beta \mu}\left(\frac{dp_l}{dz} - \rho_l g\right), \qquad z_f < z < z_0, \quad (1)$$

where R is the corner film menisci in-plane curvature radius [Fig. 1(b)], μ the liquid viscosity, and β a dimensionless resistance [9]; z_f is the film tip position ($z_f = 0$ during the CRP). Note that the curvature in the z direction, i.e., along the tube, is neglected. This, however, does not affect significantly our results because the film tip region where the axial curvature is non-negligible is in fact $O(w)$, that is quite small. The vapor transport by diffusion in the gas phase is only significant in the film tip region and can be neglected further below in the tube. We therefore assume that the phase change takes place only at the film tip. Combining Eq. (1) with Laplace's law, $p_l = p_g - \frac{\gamma}{R}$ where γ is the surface tension, leads to

$$q = \rho_l \frac{\lambda}{\beta \mu}\left(\gamma R^2 \frac{dR}{dz} - R^4 \rho_l g\right), \qquad z_f < z < z_0, \quad (2)$$

which, combined with the mass balance equation $4q = \rho_l d^2 (1 - A_c^*) \frac{dz_0}{dt}$, leads to

$$(1 - A_c^*)\frac{dz_0}{dt} = \frac{4\lambda}{d^2 \beta \mu}\left(\gamma R^2 \frac{dR}{dz} - R^4 \rho_l g\right), \qquad z_f < z < z_0. \quad (3)$$

Assuming that the bulk meniscus shape is essentially identical to the quasistatic shape yields $p_g - p_l(z_0) = \frac{3.77\gamma}{d}$ [8], and therefore $R = d/3.77$ as boundary condition at $z = z_0$. For given values of z_0 and $\frac{dz_0}{dt}$ deduced from the experimental data, Eq. (3) is solved for determining the evolution of R along the film, and then the film thickness $w = (\sqrt{2} - 1)(R - r_0)$. Contrary to a perfectly sharp corner, Eq. (3) cannot be solved analytically because the dimensionless flow resistance β depends on R for a rounded corner [9]. The degree of roundedness is an important parameter. A perfectly sharp corner would lead to a much longer CRP. A finite difference numerical solution gives the results displayed in Fig. 3, in a fairly good agreement with the experimental data. We have also plotted the thinning due to the effect of gravity forces only, a solution referred to as the purely hydrostatic one in the caption of Fig. 3 and given by $\mathrm{Bo}(z_0^* - z_f^*) = \frac{1}{R^*(z_f^*)} - \frac{1}{R(z_0^*)}$, where the * indicates a variable made dimensionless using d as characteristic length. Bo is the Bond number, $\mathrm{Bo} = \frac{\rho_l g d^2}{\gamma}$. As seen in Fig. 3, gravity effects are responsible for the film thinning over most of the CRP. However, viscous effects become very significant toward the CRP end (the film thickness ceases to follow the purely hydrostatic evolution and decreases much more abruptly). When R is about to be equal to r_0 at the tube top, we expect that the films cease to be attached to the tube top and begin to recede into the tube. This event can indeed be seen on the movie obtained from the high magnification images of tube entrance and is indicated in Figs. 2 and 3. An interesting question is whether the film depinning occurs exactly at the end of the CRP (Fig. 2) or slightly later in the FRP (Fig. 3). A related question is the nature of the CRP-FRP transition: a ''cusp'' or a softer transition. The exact shape of the curve E versus S when the evaporation rate begins to drop abruptly is, however, difficult to determine with a great accuracy from our data. To gain further insight into the CRP-FRP transition, the Laplacian problem governing the vapor transport by diffusion in the gas phase is solved numerically when the shape of the corner menisci is governed by the competition between gravity and capillary forces. The three-dimensional computational domain includes the gas phase within the tube [as illustrated in Fig. 1(c)] as well as a spherical outer domain around the tube. Numerical tests have shown that a sphere with a radius equal to $5d$ was sufficient to obtain a solution independent of the sphere radius. The FLUENT™ fluid dynamics analysis package is used to generate the computational mesh and to solve the diffusion equation. The three-dimensional shape of the corner film [as illustrated in Fig. 1(c)] is deduced from a simplified analysis of the quasistatic shape of liquid-gas interface in the tube that will be detailed elsewhere. The results, presented in the right-hand inset of Fig. 3, indicate (i) that the CRP-FRP transition coincides with the film depinning and (ii) that this transition is quite similar to the cusp transition obtained from the experimental results. The depinning is not exactly at the CRP-FRP transition in the experiments because the film depinning does not occur exactly simultaneously in the four corners. From both the simulation and the experiment it can be concluded, however, that the CRP-FRP transition essentially coincides with the film

depinning. Hence the liquid no longer reaches the entrance of the system during the FRP. The numerical results also indicate the existence of an additional very short drying period at the very beginning of the evaporation process corresponding to the transition from a flat meniscus all over the tube entrance to a curved meniscus with a depth of about one internal tube width d. This period cannot be seen experimentally because the bulk meniscus is typically located 1 or 2 mm within the tube when the experiment starts.

The simulations show that the vapor concentration gradients are only significant in the film tip region and are negligible further away within the tube, a phenomenon referred to as the diffusional screening phenomenon. Hence, the dimensionless evaporation flux $E^* = \frac{E}{Dc_e d}$ (where c_e is the equilibrium water vapor mass concentration at the liquid-gas interface and D is the vapor molecular diffusion coefficient, noting that the vapor concentration in the far field is nil here) is expected to vary essentially with the film thickness w. This is illustrated in the left-hand inset in Fig. 3. Note that the computations have been performed in the dilute limit, i.e., $c_e \ll 1$, whereas this constraint is not satisfied in the experiments with heptane ($c_e \approx 0.245$ kg/m^3) or 2-propanol ($c_e \approx 0.117$ kg/m^3). This should explain the difference between the numerical and experimental results in Fig. 3.

As seen from Fig. 3, $E^* \approx 1.3$ at depinning, which allows us to introduce the length $\zeta \approx 0.77d$ for characterizing the external mass transfer resistance. Hence the external mass transfer is equivalent to the diffusive mass transfer over a tube dry section of length ζ, that is quite short compared to tube length. This allows us to finish the description of the three main drying periods. The large (more than a 50% reduction in the flux observed at the end of CRP) and abrupt decrease in the evaporation flux observed for a variation in the main meniscus displacement of order d (this corresponds to a variation of 0.04 in saturation in Fig. 3) during the FRP is fully consistent with the fact that $\zeta \approx O(d)$. The evolution of the film tip position z_f during the FRP and the RFP can therefore be deduced from the equation $\rho_\ell(1 - A_c^*)\frac{dz_0}{dt} \approx \frac{Dc_e}{\zeta + z_f}$ and is shown in Fig. 4. The results shown in Fig. 4 were obtained from the discrete data shown in Fig. 3 (circles) after some additional data filtering. As can be seen, $z_f \propto z_0$ when the variation of the evaporation flux becomes sufficiently small. As a result, $\frac{dz_0}{dt} \propto z_0^{-1}$ when $z_f \gg \zeta$, which consistently leads to the behavior $z_0 \propto \sqrt{t}$ shown in Fig. 2 when $z_0/d > 15$. This suggests that the RFP can be defined as the period where z_f varies linearly with z_0, that is the period characterized by the behavior $z_0 \propto \sqrt{t}$. The FRP-RFP transition corresponds to the intersection of the straight line with the data curve in the inset of Fig. 2 and in Fig. 4, i.e., the moment where z_f begins to vary linearly with z_0. It could be argued that z_f varies linearly with z_0 in the RFP mainly because of gravity effects since the film's extension cannot be greater than

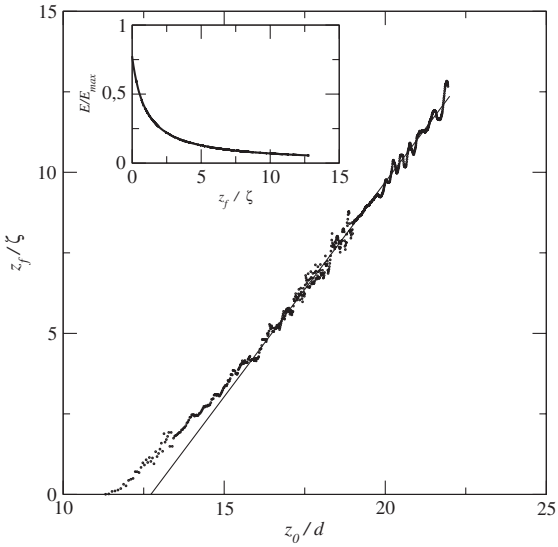

FIG. 4. Evolution of film tip position z_f in the tube as a function of z_0 for the heptane experiment. The inset shows the evolution of dimensionless evaporation flux as a function of z_f.

$(z_0^* - z_f^*)_{\max} \approx \mathrm{Bo}^{-1}(\frac{1}{r_0^*} - 3.77)$. It can be shown, however, that the regime $z_f \propto z_0$ should also be observed in the absence of gravity effects owing to viscous effects. This will be detailed in a longer paper.

Financial support from GIP ANR (Project ANR-06-BLAN-0119-01 "Intensifilm") is gratefully acknowledged.

*Corresponding author.
prat@imft.fr

[1] T. M. Shaw, Phys. Rev. Lett. **59**, 1671 (1987); M. Prat, Int. J. Multiphase Flow **19**, 691 (1993); I. N. Tsimpagnogiannis *et al.*, Phys. Rev. E **59**, 4353 (1999); M. Prat and F. Bouleux, Phys. Rev. E **60**, 5647 (1999); L. Xu *et al.*, Phys. Rev. Lett. **101**, 094502 (2008); H. Chraibi, M. Prat, and O. Chapuis, Phys. Rev. E **79**, 026313 (2009).
[2] J. B. Laurindo and M. Prat, Chem. Eng. Sci. **53**, 2257 (1998); A. G. Yiotis *et al.*, Phys. Rev. E **68**, 037303 (2003); J. C. T. Eijkel *et al.*, Phys. Rev. Lett. **95**, 256107 (2005).
[3] M. Prat, Int. J. Heat Mass Transf. **50**, 1455 (2007).
[4] T. M. Squires and S. R. Quakes, Rev. Mod. Phys. **77**, 977 (2005).
[5] J. Stefan, Akad. Wiss. Wien. **63**, 63 (1871); R. B. Bird *et al.*, *Transport Phenomena* (Wiley, New York, 1960).
[6] J. Van Brakel, in *Advances in Drying*, edited by A. S. Mujumdar (Hemisphere, New York, 1980), Vol. 1, p. 217; P. Coussot, Eur. Phys. J. B **15**, 557 (2000).
[7] A. G. Yiotis *et al.*, Water Resour. Res. **43**, W06403 (2007).
[8] H. Wong, S. Morris, and C. Radke, J. Colloid Interface Sci. **148**, 317 (1992).
[9] T. C. Ransohoff and C. J. Radke, J. Colloid Interface Sci. **121**, 392 (1988).